CARBON 77 (2014) 814–822

Available at www.sciencedirect.com

ScienceDirect

journal homepage: www.elsevier.com/locate/carbon

Microwave absorption and radiation from large-area multilayer CVD graphene

Bian Wu [a,c], Hatice M. Tuncer [b], Anestis Katsounaros [a], Weiping Wu [b], Matthew T. Cole [b], Kai Ying [b], Lianhong Zhang [a], William I. Milne [b], Yang Hao [a,*]

[a] School of Electronic Engineering and Computer Science, Queen Mary University of London, London E1 4NS, UK
[b] Department of Engineering, University of Cambridge, Cambridge CB3 0FA, UK
[c] School of Electronic Engineering, Xidian University, Xi'an 710071, PR China

ARTICLE INFO

Article history:
Received 10 February 2014
Accepted 30 May 2014
Available online 9 June 2014

ABSTRACT

Here we experimentally study the microwave absorption and near-field radiation behavior of monolayer and few-layer, large-area CVD graphene in the C and X bands. Artificial stacking of CVD graphene reduces the sheet resistance, as verified by non-contact microwave cavity measurements and four-probe DC resistivity. The multilayer stacked graphene exhibits increased absorption determined by the total sheet resistance. The underlying mechanism could enable us to apply nanoscale graphene sheets as optically transparent radar absorbers. Near-field radiation measurements show that our present few-layer graphene patches with sheet resistance more than 600 Ω/sq exhibit no distinctive microwave resonance and radiate less electromagnetic power with increasing layers; however, our theoretical prediction suggests that for samples to be practical as microwave antennas, doped multilayer graphene with sheet resistance less than 10 Ω/sq is required.

1. Introduction

As a monolayer of carbon atoms arranged in a two-dimensional honeycomb lattice, graphene is the thinnest material known to-date with high optical transparency, impressive flexibility, high electron mobility and controllable conductivity [1–3]. Considerable research has been invested in attempts to discover new applications of graphene in the THz and infrared portion of the electromagnetic spectrum. Graphene is well-suited for transparent electrodes [4], optical modulators [5], polarizers [6], plasmonic devices [7–9], photodetectors [10], hyperlenses [11], electromagnetic cloaks [12] and absorbers [13]. However, it was not until the emergence of reproducible large-area synthesis of graphene by chemical vapor deposition (CVD) did it become possible to fabricate large-scale devices with improved conductivity [14–17]. The surface conductivity and propagation properties of graphene have been analyzed rigorously [18–20]. Measurements using coplanar waveguides [21–23], rectangular waveguides [24], and cylinder resonant cavities [25–27] have been carried out to study the conductivity of graphene in the microwave regime. Graphene FET mixers [28–30], RF transistors [31–33], metasurfaces [34,35], optically transparent and dynamic controllable RF devices have all been proposed [36]. Similarly, multilayer graphene is also of great interest as a hyperbolic metamaterial in the THz regime [37].

Microwave absorption of graphene composites have been experimentally studied to design microwave absorbing mate-

* *Corresponding author.*
E-mail address: y.hao@qmul.ac.uk (Y. Hao).
http://dx.doi.org/10.1016/j.carbon.2014.05.086
0008-6223/

rial [38–40], while for the directly stacked graphene films, the microwave absorption and radiation property has not been systematically studied. Multilayer graphene is of particular interest in microwave applications: as the number of layers increases, the conductivity is enhanced. High quality multilayer graphene can be obtained by exfoliating natural graphite and isolating samples by scotch tape methods. Nevertheless, this method is irreproducible, wasteful, lacks registration potential and is impractical for large-area applications. For antenna and shielding applications, large-area multilayer graphene can be synthesised directly by CVD, however this does not consistently yield controllable numbers of layers. Alternatively, monolayer CVD graphene can be stacked artificially to improve conductivity. However, even the synthesis and reliable transfer of high quality, large scale and highly conductive monolayer CVD graphene films remains a challenge.

In this work, we assess the limits of conductivity enhancement by artificially stacking large-area monolayer CVD graphene to form well-defined and well-controlled samples of turbostratic few-layer graphene, employing a repeat transfer process which reduces the post-lift-off PMMA residue in the inter-layer cavities. We employ the microwave resonant cavity method to characterize the absorption effect of large-area graphene stacks from 1 to 5 layers, and extract their equivalent surface resistances which we compare with DC resistivity measurements. In our previous work we observed a marginally weaker near-field radiation from a monolayer graphene patch on microstrip compared with a Cu patch of the same size [41]. In the present study we demonstrate that large-area few-layer stacked graphene patches with sheet resistance of more than 0.6 kΩ/sq exhibit significantly less radiation with more layers, despite the conductivity enhancement. Here, we classify these two operation regions for CVD graphene, according to its sheet resistance, for microwave applications. Graphene, with a large sheet resistance (typically > 0.1 kΩ/sq) located in the lossy dielectric region is mainly used as an absorptive thin film, while graphene with a lower sheet resistance (typically < 0.01 kΩ/sq) in the quasi-metallic region has the potential for radiating antenna applications.

2. Experimental

2.1. CVD graphene synthesis

Graphene was grown by thermal CVD in a cold-walled, commercially available reactor (Black Magic, Aixtron Ltd.). 500-nm-thick Cu was magnetron sputtered onto 200 nm thermally oxidized Si ⟨100⟩ 4-inch wafers. Wafers were subsequently annealed at 850 °C for 30 min in a 20:1500 standard cubic centimeters per minute H_2:Ar atmosphere at 4 mbar. Graphene growth was initiated by introducing 7 sccm CH_4 (99.9%) under H_2 (99.98%) and Ar (99.998%) dilution. All samples were cooled to 300 °C under ultra-high purity N_2 (99.999%) before venting the chamber. Temperatures were monitored using two type K bimetallic thermocouples and a surface infrared interferometer. Pressures and temperatures were accurate to within ±0.1 mbar and ±1 °C, respectively.

2.2. Transfer of monolayer and stacked multilayer graphene

The graphene on Cu/SiO_2/Si wafer was diced into samples of 17 mm × 8.5 mm before casting poly (methyl methacrylate) (PMMA 950 A4) at 4000 r.p.m. for 30 s and annealing at 180 °C for 1 min. Samples were immersed in an aqueous ammonium persulfate ($(NH_4)_2S_2O_8$) etchant (2.2 g/100 mL DI) for 12 h to etch the Cu catalyst. The floating PMMA-graphene films were transferred into DI water baths using a microscope glass slide and rinsed several times to remove the etchant and residual contaminants. For monolayer graphene, the PMMA-graphene film was transferred on to optical fused quartz substrate (24.6 mm in diameter and 1.25 mm in thickness), which was subsequently dried at atmospheric pressure for 24 h. For monolayer samples the films were transferred to occupy only one half of the quartz substrates, leaving the other half side exposed for UV–Vis spectrometry baseline calibration purposes. For multilayer samples the films were transferred onto slightly larger diced wafer substrate pieces, in order to make PMMA/bilayer graphene stacks. The bilayer stacked substrates were etched again in $(NH_4)_2S_2O_8$ and some of the films were rinsed and transferred onto target quartz substrates, followed by acetone lift-off to remove the PMMA to make bilayer graphene samples. The rest of the PMMA/bilayer graphene films were transferred again onto larger diced substrates and the process was repeated until stacked samples of up to 5 layers were processed.

2.3. Characterization

The optical transmittance of the samples was measured from 200 nm to 1000 nm using a UV–Vis Spectrophotometer. Baselines were calibrated without a substrate, in air, followed by the measurements of bare quartz, monolayer and few-layer samples. The Raman spectroscopy was performed on the as-grown graphene on the Cu/SiO_2/Si growth wafer with an incident power < 3 mW and a spot size less than 1 μm. The transferred monolayer and multilayer graphene were measured at 457 nm (2.71 eV), 532 nm (2.33 eV) and 633 nm (1.96 eV) (see Fig. S1a–d). The DC resistivity was measured using a four-point probe contact stylus. The Keithley Model 2100/120 Digital Multimeter with a four-point probe was calibrated with an indium tin oxide coated quartz substrate prior to the measurements. A minimum of thirteen measurements, at different locations, were taken to characterize the resistivity spatial distribution.

2.4. Microwave resonant cavity measurement

A microwave resonant cavity approach was used to measure the forward transmission response and the quality factor with and without the few-layer graphene (see Fig. S2). The Cu cylindrical cavity, with a radius R of 26 mm and height H of 40 mm, resonates in the TE_{111} mode at 5.051 GHz. Two 1 mm length probes with SMA connectors located at one and three quarters of the cavity height provide the weak-coupled external excitation. The cavity was split into two parts across the cylinder center to allow for sample

placement. The two ports of an Agilent N5230 PNA-L Network Analyser were connected to the SMA probes of the cavity *via* screened coaxial cables and a PNA-L calibrated across a narrow frequency range from 5.049 GHz to 5.053 GHz in 1 MHz steps.

2.5. *Microwave near-field measurement*

A near field scanner (NSI-200V) was employed to scan the electromagnetic field distribution across the graphene samples (see Fig. S4). The samples under test were attached onto microstrip lines on Duroid substrates and mounted vertically on a polystyrene support for rigidity. The transmitting port of the PNA-L Network Analyzer was connected to the microstrip line *via* an SMA connector and a screened cable. The near-field radiation pattern was detected by a monopole probe connected to the receiving port of the PNA-L *via* a 3 m screened cable. The surface of the sample under test was scanned vertically and horizontally at a height of 1 cm to measure the near-field radiation at the XOZ and YOZ planes at 5 GHz and 8 GHz. The near-field amplitude and phase data were obtained using the software NSI2000.

3. Results and discussion

3.1. *Sample preparation and characterization results*

Monolayer graphene was synthesised by thermal CVD. Samples were diced from 4 inch graphene/Cu (1 μm)/SiO_2 (200 nm)/Si wafers and transferred on to fused silica quartz substrates using a 200 nm thick PMMA as the supporting polymer. The stacking method involved repetitively transferring the PMMA-graphene films onto diced graphene/Cu/SiO_2/Si substrates and etching the underlying Cu catalyst in 2.2% w/v ammonium persulfate solution for 12 h, before transferring the graphene/PMMA onto the target quartz substrates (Fig. 1a). This method avoids the accumulation of deleterious PMMA residues between the graphene layers, which can be only partially removed by aggressive thermal annealing and repeated acetone baths. One to 5 layer (5L) graphene samples were prepared in this fashion.

Suspended monolayer graphene has an opacity of 2.3 ± 0.1% [42]. UV–Vis optical transmittance confirmed the number of the stacked graphene samples (Fig. 1b), which were consistent with the number of transfer steps undertaken, supporting our *in situ* Raman data which indicated monolayer as-grown graphene. The 1.27 mm thick Spectrosil fused silica quartz substrate had >90% transmission throughout the probed optical window (200–1000 nm). Monolayer and few-layer stacked samples showed characteristic absorption from 250 nm to 300 nm, and almost uniform absorption from 600 nm to 1000 nm which increases with the number of layers. The 5L sample absorbs only 0.7% more than the 4L sample, suggesting this sample is more likely a partial 4L with some regions of 5L.

Polychromatic Raman spectroscopy revealed that the transferred monolayer graphene had an I_D/I_G ratio of ~ 0.17 (±0.02) and an I_{2D}/I_G ratio ~ 3.0 (±0.12) (see Fig. S1a). The multilayer Raman peak modes are plotted at all laser energies (Fig. S1b–d). A comparison of the I_D/I_G and I_{2D}/I_G ratios (Fig. S1e, f) shows a decreasing trend up to 4L after which there is a slight increase. Peak mode analysis reveals a 7 cm^{-1} red-shift in the G band for 5L compared to the monolayer case, which might be attributed to doping [43]. The maximum D band peak for the 5L blue shifts by 9 cm^{-1} relative to the monolayer samples. The multilayer 2D bands are single peaks which can be fitted by single Lorentzian functions, with FWHMs up to 47 cm^{-1} for the 5L case. The 2D band peak blue shifts by a maximum of 10 cm^{-1} and its intensity increases by up to 56% as the number of layers increase from 1L to 5L, suggesting *p*-type doping.

3.2. *Microwave resonant cavity absorption of multilayer graphene*

Microwave cavity absorption techniques allow the determination of graphene resistivity without having to physically vapor deposit metal contact electrodes for Van der Pauw measurements or requiring the use of stylus contact probes. The principle of operation is similar to the millimeter-wave method of extracting sheet resistance by measuring power transmission through thin films where the source and power

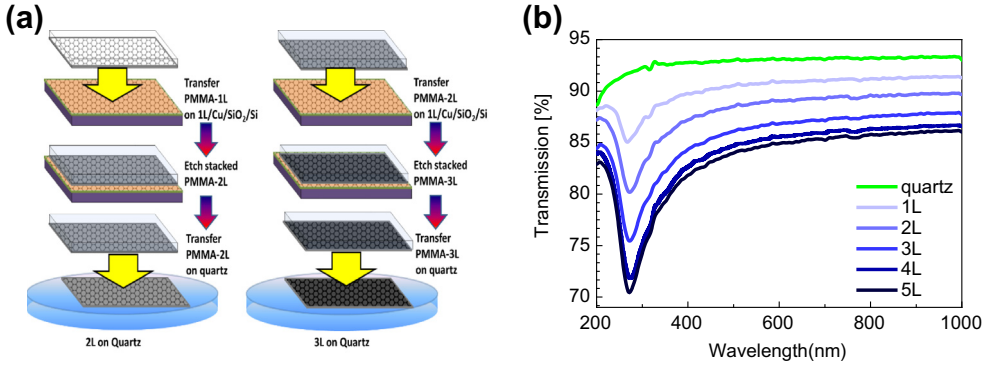

Fig. 1 – (a) Schematic illustration of the multi-step transfer-and-etch cycle for 2L and 3L stacked graphene, (b) UV–Vis spectroscopy optical transmittance measurements for bare quartz, monolayer and 2–5L stacked graphene on quartz. (A colour version of this figure can be viewed online.)

meter are coupled through dielectric waveguides [27]. The microwave cavity method has been successfully adopted elsewhere to extract sheet resistances of epitaxial graphene and graphene oxide [25,26]. Here, we utilize a simple microwave cylindrical cavity method which is suitable for large-area samples and is implemented by directly loading the graphene-quartz samples at the cavity base (Fig. 2a and Fig. S2a, b). The cylindrical cavity, of height H and radius R, is excited by a pair of probes located at $H/4$ and $3H/4$, through weak coupling. The graphene bearing quartz substrate, placed at the base, behaves as a Salisbury screen-like absorber which suppresses both the transmission coefficient and the quality factor. This effect increases as the conductivity of the graphene improves with increased number of layers. The cavity resonates in the TE_{111} mode at $f_0 = c\sqrt{(1/3.412R)^2 + (1/2H)^2} \approx 5.051$ GHz, where c is the speed of light in vacuum. When a bare quartz substrate is placed at the base of cavity the resonance frequency shifts to a lower frequency f_0' due to the dielectric perturbation.

For monolayer graphene on quartz, the transmission responses show a suppressed resonance peak and an increased 3 dB-bandwidth of $BW_{3dB} = f_R - f_L$, while the total quality factor of the cavity represented by $Q_t = f_0'/BW_{3\,dB}$ is reduced (Fig. 2b). A 2L graphene on quartz loading achieves a dramatic peak suppression of about 10 dB, followed by a slowly increasing suppression from 3L to 4L. Interestingly, the 5L sample does not enhance suppression any further, and it behaves as per the 4L sample, as shown in the above optical transmittance measurements.

In the microwave regime, the complex resistivity of graphene has a constant real term (resistance) and negligible reactance [18,19]. Thus, the sheet resistance obtained at a single frequency using our microwave cavity approach may represent a wideband resistivity. The dependence of the quality factor or resonance peak of the graphene-loaded cavity on the sheet resistance is obtained from Ansys HFSS full-wave electromagnetic simulations as shown in Fig. 2c. The total quality factor of the graphene-loaded cavity can also be defined as $Q_t = 1/(1/Q_c + 1/Q_q + 1/Q_g)$, where Q_c, Q_q, Q_g represent the quality factor of the cavity, quartz and graphene, respectively. The minimum quality factor (or the minimum resonance peak) corresponds to the maximum absorption point at R_{s0}. For $R_s < R_{s0}$, graphene behaves as a quasi-metallic material with its quality factor inversely proportional to the sheet resistance; whilst for $R_s > R_{s0}$, graphene behaves like a lossy dielectric with the quality factor proportional to the sheet resistance. Here, we label the two regions as 'quasi-metallic' and 'lossy dielectric', respectively. In the lossy dielectric region the measured resonance peaks and quality factors decrease with increasing layer number.

The sheet resistance of multilayer graphene is extracted by curve fitting the measured and simulated transmission responses. Fig. 2d shows that the extracted sheet resistance from the microwave cavity measurements falls sharply from 5.26 kΩ/sq, for monolayer graphene, to 1.1 kΩ/sq, for 2L

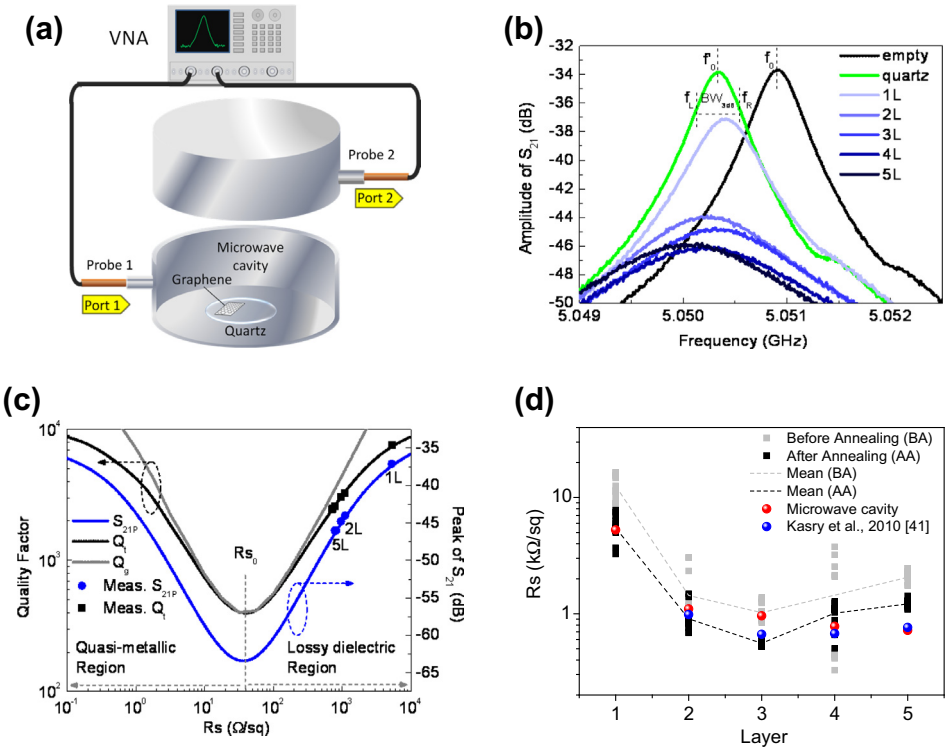

Fig. 2 – (a) Microwave cavity measurement set-up, (b) measured transmission spectra of graphene-loaded microwave cavity, (c) predicted and measured quality factor and resonance peak relationship with sheet resistance. R_{s0} is the maximum absorption point which is chosen as a boundary for two operation regions, (d) a comparison of DC sheet resistance (before and after annealing) and microwave cavity measurement of this work with DC sheet resistance of multilayer graphene before doping by Kasry et al. [44]. (A colour version of this figure can be viewed online.)

graphene, then incrementally decreases from 0.96 kΩ/sq for 3L to 0.72 kΩ/sq for 5L, which shows the monotonically decreased sheet resistance with number of layers. The drop is significant from 1L to 2L while less so for the following layers.

3.3. DC sheet resistance of multilayer graphene

The DC sheet resistance was assessed using conventional contact stylus four-probe approaches, as shown in Fig. 2d. The sheet resistance values measured at various spots on the monolayer samples were very inhomogeneous and range from 8.8 kΩ/sq to 17 kΩ/sq, (1σ = 3 kΩ/sq). The 2L stacked graphene showed improvement in conductivity to a minimum of 0.9 kΩ/sq with a maximum of 3 kΩ/sq. The conductivity of the 3L samples did not vary as much (1σ = 0.2 kΩ/sq) and the minimum value of the sheet resistance fell to 0.8 kΩ/sq. The 4L samples measured at some spots improved to 0.3 kΩ/sq but the values varied greatly rising to as much as 3.8 kΩ/sq. The 5L sample has a minimum of 1.3 kΩ/sq. It is interesting to observe that after 3L, as the layer number increases the sheet resistance tended to deviate more across the sample, especially in the 4L case (1σ = 1.3 kΩ/sq).

The DC mean sheet resistivity for the 1–5L samples were 12.6, 1.4, 1, 1.5 and 2.1 kΩ/sq, respectively. These average values are high and do not show a monotonic decrease after 3L as found in the microwave extracted results. This is most likely due to the partial contact between layers and the additive presence of dopants, such as the residual etchant and water molecules between the higher number layers. We verified the latter by vacuum annealing the samples to remove the trapped dopants and any chemicals accumulated by handling during the experiments. Samples were annealed at 5 mbar at 320 °C for 30 min. Sheet resistance measurements were consistently conducted on samples 30 min after the annealing process.

Measurements revealed that annealing improved the overall homogeneity considerably. Mean values for 1–5L samples were 5.5, 0.9, 0.6, 1 and 1.2 kΩ/sq. Annealing reduced the monolayer graphene sheet resistance 1σ variation by 59% and the maximum value to 7.7 kΩ/sq, while improving the minimum to 3.3 kΩ/sq. The homogeneity improvement increased with layer numbers, with the most dramatic improvement for the 4L graphene as 1σ reduced by 82% to 0.2 kΩ/sq. The maximum resistance values were reduced by a consistent average of 53% across all samples. Interestingly, upon annealing, the mean DC sheet resistances were similar to the microwave cavity extracted values as shown in Fig. 2d. Despite these improvements, 4L and 5L samples still do not show a monotonic decrease from the 3L value as anticipated.

DC measured results reported by Kasry et al. [44], who use a layer-by-layer transfer method, also show a small increase from 3L (666 Ω/sq) to 4L (674 Ω/sq) and 5L (763 Ω/sq), (Fig. 2d). For higher number of layers, the DC sheet resistance decreases monotonically after 5 layers. In this work, we have used the same PMMA scaffolding, as we stacked up layers of graphene and removed the PMMA after the transfer on to the quartz substrate. Despite the differences in transfer methods, the resistance values follow a similar trend. For our monolayer annealed samples the 95% confidence interval is 5.47 ± 0.63 kΩ/sq. By annealing we have partially removed the *p*-type interlayer dopants and any organic build-up or remaining PMMA residue on the top layer.

3.4. Microwave near-field radiation from multilayer graphene

In order to assess the influence of the number of graphene layers on microwave near-field radiation, monolayer and multilayer graphene samples were placed on a 50 Ω microstrip line and treated as a capacitively coupled patch antenna. The microstrip line was on a 1.57 mm thick, 60 mm × 40 mm Duroid substrate (ε_r = 2.2). The monopole probe was placed in the XOY plane and parallel to the microstrip feed line (Fig. 3a, Fig. S4). The measured reflection coefficients of the microstrip-coupled graphene patch was compared with the bare quartz case, as illustrated in Fig. 3b. The monolayer graphene has a slightly suppressed reflection relative to the bare quartz due to its high sheet resistance (5.3 kΩ/sq), making both the absorption and radiation effects negligible.

Similar to the microwave cavity measurement, 2L graphene also showed a prominent suppression of reflection from 2 GHz to 14 GHz, and then the 3–5L showed a less obvious reduction. However, full-wave simulations predict a resonance effect as a patch antenna only in the quasi-metallic region, i.e. $R_s < R_{s0}$. Resonance occurs at 8 GHz when the graphene patch was center-coupled to the microstrip line and at 7.4 GHz when it is edge-coupled (Fig. S5). The low sheet resistance (typically < 0.01 kΩ/sq) required for microwave resonance suggest that a further conductivity improvement for the graphene film is needed to realize a practical microwave graphene patch antenna. The absorptive behavior of the lossy graphene patch leads to a reduction of the radiation efficiency compared to a Cu patch antenna in the far-field. Near-field measurements were conducted to study the radiation properties of multilayer graphene. In Fig. 4, the normalized radiation amplitudes of monolayer and multilayer graphene at the XOZ and YOZ cross-section planes, at 5 GHz and 8 GHz, are given. Bare quartz was used as a reference.

At 5 GHz, the normalized near-field radiation from the multilayer graphene and quartz are symmetrical around the XOZ plane. However, all the graphene-quartz samples have reduced radiation with respect to the bare quartz. For an increased number of layers, absorption increases due to reduced sheet resistance in the lossy dielectric region resulting in a further reduction in radiation (Fig. 4a). The same trend was also noted at the YOZ plane, except for an asymmetrical distribution along the Y-direction, with the peak radiation shifting to Y = 15 mm as a result of the coupling effect from the microstrip feed line (Fig. 4b).

At 8 GHz, the symmetrical field distribution also exists in the XOZ plane, but the peak shift from the center is smaller in the YOZ plane, as shown in Fig. 4c and d. The difference in the radiation amplitude for multilayer graphene becomes more apparent and manifests as decreased near-field radiation with increased layers. This is due to increased absorption when the sheet resistance is still in the lossy dielectric region. In this case, the resistive multilayer graphene patch, backed with the ground plane and separated by the substrates, forms an absorber rather than a radiating

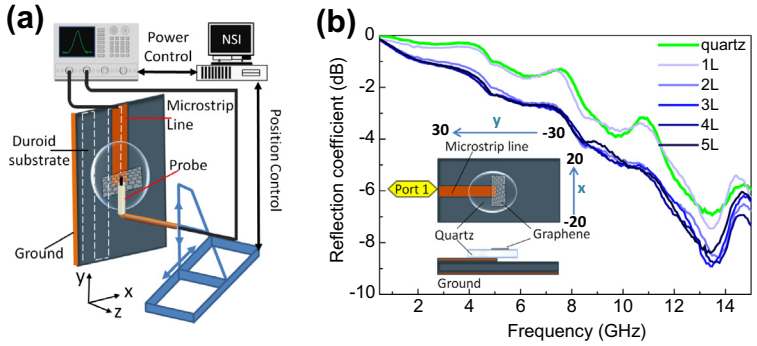

Fig. 3 – (a) Schematic of near-field radiation measurement set-up. (b) Measured reflection coefficients of multilayer graphene patches (1–5L) on quartz fed by a 50 Ω microstrip line, showing decreased reflection from 1L to 5L and no distinct resonance. (A colour version of this figure can be viewed online.)

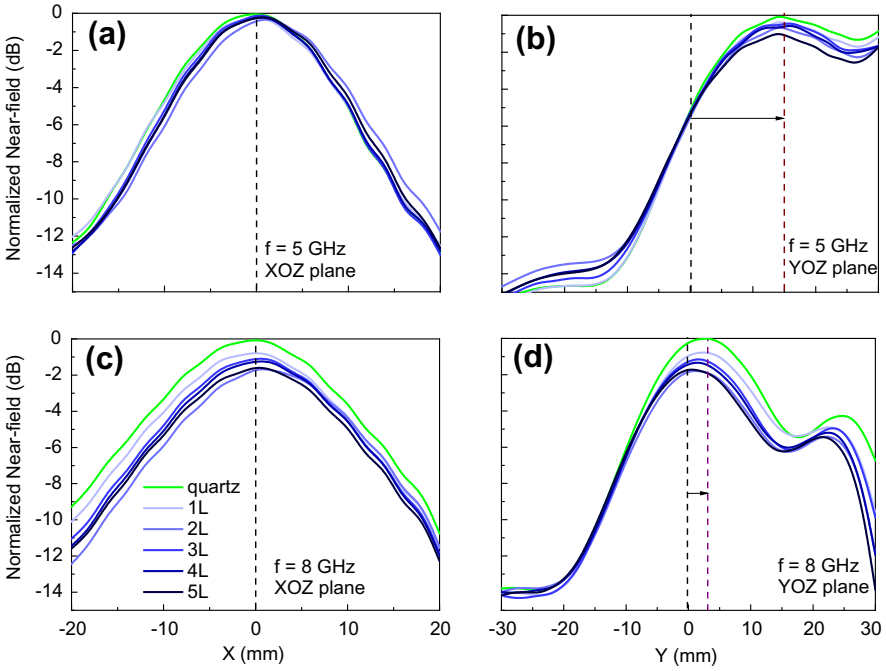

Fig. 4 – (a and b) Normalized near-field amplitudes of multilayer graphene patches (1–5L) on quartz in the XOZ and YOZ planes at 5 GHz, both show that graphene patch is radiating slightly less than the bare quartz and more layers radiate less when Y > 0 mm. (c and d) Normalized near-field amplitudes in the XOZ and YOZ planes at 8 GHz, showing a smaller shift of radiation peak from the center, and evidently less radiation for more layers. (A colour version of this figure can be viewed online.)

antenna. Thus, we observe increased absorption when the sheet resistance of graphene shifts towards R_{s0} as the layers increase from 1L to 5L.

In Fig. 5 we illustrate the measured near-field radiation patterns for the 1L, 3L and 5L graphene on quartz and also for bare quartz. At 5 GHz the graphene patches with increasing number of layers radiate less (Fig. 5a). At 8 GHz, the coupling effect of the microstrip line is weakened and the position of peak near-field radiation for quartz and multilayer graphene shifts from Y = 15 mm to Y = 0 mm (Fig. 5b). Meanwhile, the radiation amplitude also evidently decreases for more layers with respect to bare quartz.

Since graphene is lossy at microwave frequencies, its absorption will affect the radiation properties of the patch strongly. Full-wave simulations of the far-field radiation indicate that the radiation peak gain in the lossy dielectric region is even less than −5 dBi, much less than that of 6 dBi from a Cu patch of the same geometry, and a little less than the bare quartz case (Fig. S6). This suggests that the graphene patch with a large sheet resistance behaves like an absorber rather than an antenna, as validated in the previous near-field measurement. However, for low sheet resistance (R_s < 10 Ω/sq) in the quasi-metallic region the peak gain of the graphene patch increases to an acceptable level (>0 dBi), which can be realized by further doping or electrical biasing. In this case, the graphene patch may find applications in transparent and flexible radiating antenna with improved radiation efficiency relative to incumbent technologies.

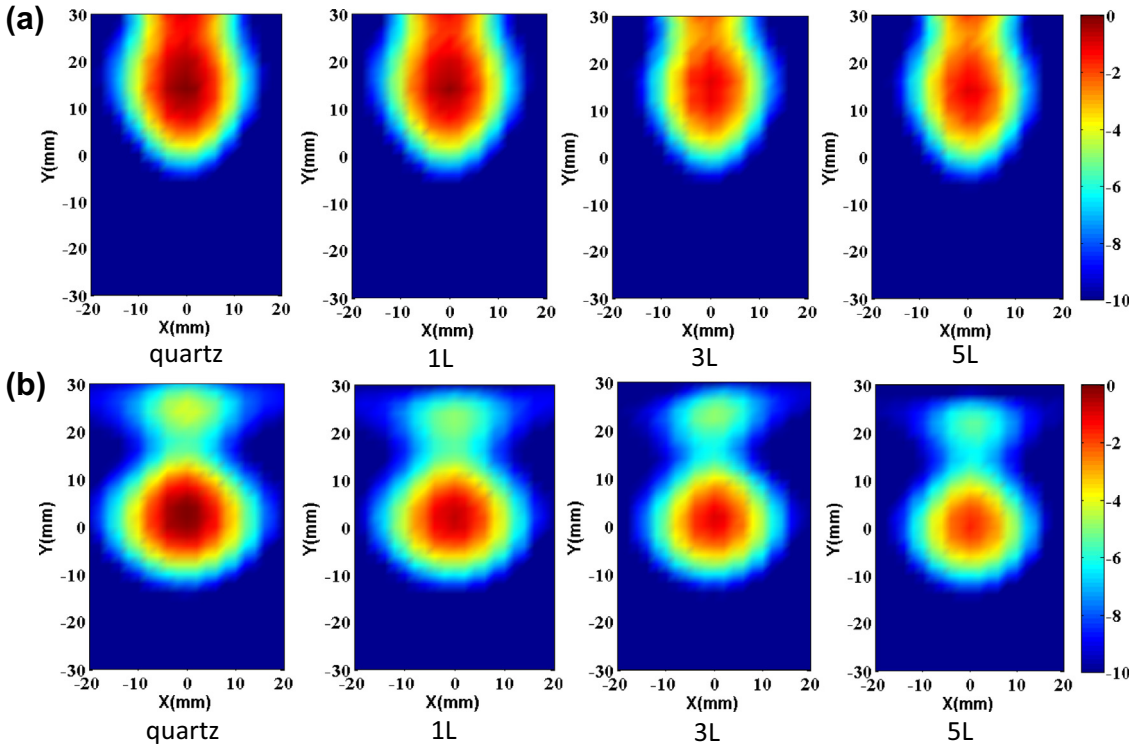

Fig. 5 – (a) Measured near-field radiation patterns of multilayer graphene patches on quartz at 5 GHz. The graphene patch with an increasing number of layers has decreasing radiation, and even less than that of bare quartz. (b) Measured near-field radiation patterns at 8 GHz. The radiation peaks are located at the patch center and the intensity is reduced for increasing layers. (A colour version of this figure can be viewed online.)

4. Conclusions

Microwave absorption and radiation measurements were carried out with the aim of assessing the suitability of multilayer graphene for microwave applications. Our microwave cavity measurements validate that both the resonance peak and the quality factor are reduced by the increased conductivity exhibited by multilayer stacked graphene. The inherently absorptive behavior of the ultra-thin resistive graphene film material can be used to design flexible, optically transparent microwave absorbers, where consecutive stacking of the graphene-dielectric layers above a conductive ground or inside a shielding package, is used to suppress unwanted resonance. The multilayer graphene films could achieve a wide range of sheet resistance values for the desired impedance matching condition of the absorber, and shows much potential if coupled to wet-chemical doping protocols.

Near-field measurements revealed that increasing the number of graphene layers at the lossy dielectric region does not enhance radiation; instead, the radiation amplitude decreases due to increased absorption. In order to improve the radiation as a patch antenna, lower sheet resistivity graphene in the quasi-metallic region is required. For $R_s < 10\ \Omega$/sq, the far-field radiation gain of a graphene patch at resonant frequency can be larger than 0 dBi and it continues to increase with decreasing R_s. Although current experimental work includes only large sheet resistances and present few-layer graphene patches do not achieve the antenna performance, if the sheet resistance is highly reduced by doping or electrical biasing, they can be used as optically transparent and mechanically flexible microwave antennas.

Acknowledgements

This work was funded by the Graphene Research Centre, University of Cambridge, and the Engineering and Physical Sciences Research Council (EPSRC), UK under a Program Grant (EP/K01711X/1). M.T.C. thanks the Winston Churchill Trust and the International Young Scientist Research Fellowship, National Natural Science Foundation of China, for generous financial support. B.W. acknowledges the fund support from the China Scholarship Council and National Natural Science Foundation of China No. 61271017. H.M.T. thanks Dr I. Lestas for discussions on statistical analysis. We thank the Cavendish Laboratories, Cambridge University, for granting access to their Raman Spectrometer.

Appendix A. Supplementary data

Supplementary data associated with this article can be found, in the online version, at http://dx.doi.org/10.1016/j.carbon.2014.05.086.

REFERENCES

[1] Geim AK, Novoselov KS. The rise of graphene. Nat Mater 2007;6(3):183–91.
[2] Geim AK. Graphene: status and prospects. Science 2009;324(5934):1530–4.
[3] Novoselov KS, Fal VI, Colombo L, Gellert PR, Schwab MG, Kim K. A roadmap for graphene. Nature 2012;490(7419):192–200.
[4] Bae S, Kim H, Lee Y, Xu X, Park JS, Zheng Y, et al. Roll-to-roll production of 30-inch graphene films for transparent electrodes. Nat Nanotechnol 2010;5(8):574–8.
[5] Liu M, Yin X, Ulin-Avila E, Geng B, Zentgraf T, Ju L, et al. A graphene-based broadband optical modulator. Nature 2011;474(7349):64–7.
[6] Bao Q, Zhang H, Wang B, Ni Z, Lim CHYX, Wang Y, et al. Broadband graphene polarizer. Nat Photon 2011;5(7):411–5.
[7] Fei Z, Rodin AS, Andreev GO, Bao W, McLeod AS, Wagner M, et al. Gate-tuning of graphene plasmons revealed by infrared nano-imaging. Nature 2012;487(7405):82–5.
[8] Tamagnone M, Gómez-Díaz JS, Mosig JR, Perruisseau-Carrier J. Reconfigurable THz plasmonic antenna concept using a graphene stack. Appl Phys Lett 2012;101:214102.
[9] Ju L, Geng B, Horng J, Girit C, Martin M, Hao Z, et al. Graphene plasmonics for tunable terahertz metamaterials. Nat Nanotechnol 2011;6(10):630–4.
[10] Gabor NM, Song JC, Ma Q, Nair NL, Taychatanapat T, Watanabe K, et al. Hot carrier–assisted intrinsic photoresponse in graphene. Science 2011;334(6056):648–52.
[11] Andryieuski A, Lavrinenko AV, Chigrin DN. Graphene hyperlens for terahertz radiation. Phys Rev B 2012;86(12):121108.
[12] Chen PY, Alù A. Atomically thin surface cloak using graphene monolayers. ACS Nano 2011;5(7):5855–63.
[13] Andryieuski A, Lavrinenko A. Graphene metamaterials based tunable terahertz absorber: effective surface conductivity approach. Opt Express 2013;21(7):9144–55.
[14] Kim KS, Zhao Y, Jang H, Lee SY, Kim JM, Kim KS, et al. Large-scale pattern growth of graphene films for stretchable transparent electrodes. Nature 2009;457(7230):706–10.
[15] Reina A, Jia X, Ho J, Nezich D, Son H, Bulovic V, et al. Large area, few-layer graphene films on arbitrary substrates by chemical vapor deposition. Nano Lett 2009;9(1):30–5.
[16] Li X, Zhu Y, Cai W, Borysiak M, Han B, Chen D, et al. Transfer of large-area graphene films for high-performance transparent conductive electrodes. Nano Lett 2009;9(12):4359–63.
[17] Li X, Cai W, An J, Kim S, Nah J, Yang D, et al. Large-area synthesis of high-quality and uniform graphene films on copper foils. Science 2009;324(5932):1312–4.
[18] Hanson GW. Dyadic Green's functions and guided surface waves for a surface conductivity of graphene. J Appl Phys 2008;103(6):064302.
[19] Hanson GW. Dyadic Green's functions for an anisotropic non-local model of biased graphene. IEEE Trans Antennas Propag 2009;56(3):747–57.
[20] Deligeorgis G, Dragoman M, Neculoiu D, Dragoman D, Konstantinidis G, Cismaru A, et al. Microwave propagation in graphene. Appl Phys Lett 2009;95(7):073107.
[21] Skulason HS, Nguyen HV, Guermoune A, Sridharan V, Siaj M, Caloz C, et al. 110 GHz measurement of large-area graphene integrated in low-loss microwave structures. Appl Phys Lett 2011;99(15):153504.
[22] Dragoman M, Neculoiu D, Cismaru A, Muller AA, Deligeorgis G, Konstantinidis G, et al. Coplanar waveguide on graphene in the range 40 MHz–110 GHz. Appl Phys Lett 2011;99(3):033112.
[23] Wu Y, Xu Y, Wang Z, Xu C, Tang Z, Chen Y, et al. Microwave transmission properties of chemical vapor deposition graphene. Appl Phys Lett 2012;101(5):053110.
[24] Gomez-Diaz JS, Perruisseau-Carrier J, Sharma P, Ionescu A. Non-contact characterization of graphene surface impedance at micro and millimeter waves. J Appl Phys 2012;111(11):114908.
[25] Krupka J, Strupinski W. Measurements of the sheet resistance and conductivity of thin epitaxial graphene and SiC films. Appl Phys Lett 2010;96(8):082101.
[26] Hao L, Mattevi C, Gallop J, Goniszewski S, Xiao Y, Cohen L, et al. Microwave surface impedance measurements on reduced graphene oxide. Nanotechnology 2012;23(28):285706.
[27] Collier RJ, Hasko DG. Measurement of the sheet resistance of resistive films on thin substrates from 120 to 175 GHz using dielectric waveguides. J Appl Phys 2002;91(4):2547–9.
[28] Wang H, Hsu A, Wu J, Kong J, Palacios T. Graphene-based ambipolar RF mixers. IEEE Electron Device Lett 2010;31(9):906–8.
[29] Lin YM, Valdes-Garcia A, Han SJ, Farmer DB, Meric I, Sun Y, et al. Wafer-scale graphene integrated circuit. Science 2011;332(6035):1294–7.
[30] Habibpour O, Vukusic J, Stake J. A 30-GHz integrated subharmonic mixer based on a multichannel graphene FET. IEEE Trans Microw Theory Tech 2013;61(2):841–7.
[31] Lin YM, Jenkins KA, Valdes-Garcia A, Small JP, Farmer DB, Avouris P. Operation of graphene transistors at gigahertz frequencies. Nano Lett 2009;9(1):422–6.
[32] Schwierz F. Graphene transistors. Nat Nano 2010;5(7):487–96.
[33] Dragoman M, Neculoiu D, Dragoman D, Deligeorgis G, Konstantinidis G, Cismaru A, et al. Graphene for microwaves. IEEE Microw Mag 2010;11(7):81–6.
[34] Fallahi A, Perruisseau-Carrier J. Design of tunable biperiodic graphene metasurfaces. Phys Rev B 2012;86(19):195408.
[35] Padooru YR, Yakovlev AB, Kaipa CS, Hanson GW, Medina F, Mesa F. Dual capacitive-inductive nature of periodic graphene patches: transmission characteristics at low-THz frequencies. Phys Rev B 2013;87(11):115401.
[36] Chamanara N, Sounas D, Szkopek T, Caloz C. Optically transparent and flexible graphene reciprocal and nonreciprocal microwave planar components. IEEE Microw Wireless Compon Lett 2012;22(7):360–2.
[37] Iorsh IV, Mukhin IS, Shadrivov IV, Belov PA, Kivshar YS. Hyperbolic metamaterials based on multilayer graphene structures. Phys Rev B 2013;87(7):075416.
[38] Singh VK, Shukla A, Patra MK, Saini L, Jani RK, Vadera SR, et al. Microwave absorbing properties of a thermally reduced graphene oxide/nitrile butadiene rubber composite. Carbon 2012;50(6):2202–8.
[39] Goyal RK. Cost-efficient high performance polyetheretherketone/expanded graphite nanocomposites with high conductivity for EMI shielding application. Mater Chem Phys 2013;142(1):195–8.
[40] Wu B, Tuncer HM, Naeem M, Yang B, Cole MT, Milne WI, et al. Experimental demonstration of a transparent graphene millimetre wave absorber with 28% fractional bandwidth at 140 GHz. Sci Rep 2014;4:4130. http://dx.doi.org/10.1038/srep04130.
[41] Katsounaros A, Cole MT, Tuncer HM, Milne WI, Hao Y. Near-field characterization of chemical vapor deposition graphene in the microwave regime. Appl Phys Lett 2013;102:233104.

[42] Nair RR, Blake P, Grigorenko AN, Novoselov KS, Booth TJ, Stauber T, et al. Fine structure constant defines visual transparency of graphene. Science 2008;320(5881):1308.
[43] Casiraghi C. Doping dependence of the Raman peaks intensity of graphene close to the Dirac point. Phys Rev B 2009;80(23):233407.
[44] Kasry A, Kuroda MA, Martyna GJ, Tulevski GS, Bol AA. Chemical doping of large-area stacked graphene films for use as transparent, conducting electrodes. ACS Nano 2010;4(7):3839–44.